Flomeko 2000 - IMEKO TC9 Conference
Salvador, Bahia, BRAZIL
4-8 June, 2000

EFFECTS OF DISTURBED INFLOW ON ACCURACY OF VORTEX-SHEDDING FLOWMETERS

S. Perpéet, E. von Lavante, H. Windorfer, V. Hans
Institute of Turbomachinery
Institute of Measurement and Control
University of Essen, Essen, Germany

Abstract: Vortical flows are mostly considered as disturbances, however, in a vortex-shedding flowmeter controlled vortex shedding from a bluff body is used for throughflow metering. In this case, any additional vortices, swirl, or pulsations introduced upstream will interfere with the meter's function. In the present work, the effect of inflow vortices on the accuracy and function of a vortex-shedding flowmeter are investigated numerically. The inflow vortices are induced by a single and double bend positioned upstream of the bluff body. The resulting flow is analyzed using visualization and DFT for various types of bluff bodies.

Keywords: Vortex-shedding flowmeter, Disturbed inflow, Bends

1 INTRODUCTION

Many aerodynamic problems require a volume- or mass-flow data for its quantitative solution. Therefore, a number of methods for flow rate measurement have been developed. One relatively simple and promissing flow measurement device is the so-called vortex shedding flowmeter, in which the mass flow is determined by observing relationship between the vortex-shedding frequency from a bluff body, attached inside channel, and the corresponding mean velocity about it. The bluff body causes production of a system of periodic vortices, whose frequency can be correlated with the mean flow velocity and, therefore, the measured mass flow. This procedure assumes a regular and well defined vortex structure as well as shedding mechanism, resulting mostly in linear dependency of the mass flow on the shedding frequency over a wide range of Reynolds numbers. However, it has been observed that certain types of disturbancies in the inflow result in rather irregular pressure signatures of the vortex system or even shift of its charachteristic frequencies, leading to unreliable mass flow data. A schematic picture of a typical vortex shedding flowmeter is offered in Figure 1.

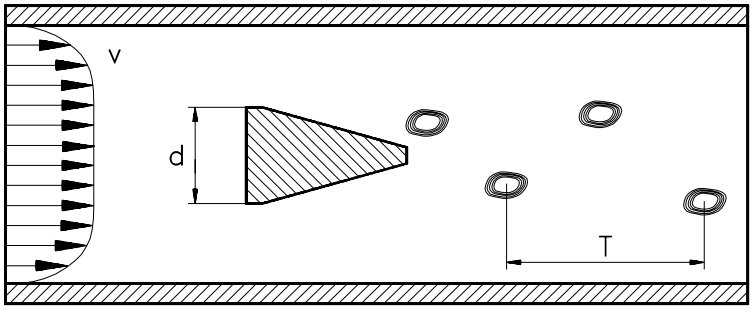

Figure 1. Principle of a vortex-shedding flowmeter.

Commercial flowmeters use a large variety of bluff body shapes, often restricted by the attachment of the pressure sensors or, more likely, patent laws. Previous application of some current bluff body designs lead to fairly irregular pressure signatures, making them unreliable. It was, therefore, decided to investigate not only the known bluff body shapes, but also a few alternate designs, developed empirically by the present authors.

In the past, various shapes of vortex bodies have been tested with regard to their applicability to a simple signal processing. Triangular shapes (Johnson [6], Fureby [2] and Madabhushi et. al. [7]) as well as shapes with truncated tips (e. g. Hans et. al. [3]) have been tested. In the preliminary part of this work, tests were performed with T-shaped, rectangular and a new-designed bluff body [15].

Well-defined vortices were generated, giving, after signal processing, excellent measurement results. A strong and well-defined dependency of the vortex frequency on the flow velocity and, therefore, the Reynolds number, could be obtained [15].

2 NUMERICAL ALGORITHM

The numerical algorithm employed uses the three-dimensional, time-dependent full Navier-Stokes equations describing the conservation of mass, momentum and energy of fluid flow. The divergence form in body-fitted, curvilinear coordinates is:

$$\frac{\partial Q}{\partial \tau} + \frac{\partial (F - F_v)}{\partial \xi} + \frac{\partial (G - G_v)}{\partial \eta} + \frac{\partial (H - H_v)}{\partial \zeta} = 0, \tag{1}$$

with $Q = J^{-1}(\rho \;\; \rho u \;\; \rho v \;\; \rho w \;\; e)^T$ the vector of the conserved variables. J is the Jacobian of the coordinates transformation from physical (x, y, z, t) to computational (ξ, η, ζ, τ) space. The program is based on the finite-volume formulation, using a cell-centered organization of the control-volumes. The spatial discretization is carried out with help of Roe's Flux Difference Scheme, a Godunov-type method providing an approximate solution of the Riemann problem on the cell interfaces. Here, the flux is [11]:

$$F_{i+\frac{1}{2}} = \frac{1}{2}\left\{ F(Q)_L + F(Q)_R + \left| \tilde{A}_{i+\frac{1}{2}} \right| (Q_R - Q_L) \right\}. \tag{2}$$

The index $i + \frac{1}{2}$ describes the values on the cell interfaces, R and L the values right and left from it. The Roe-averaged matrix $\tilde{A}$ is given by the differentiation of the local-linearized function $F(Q)$. This scheme is formally a central difference type plus a damping term. The method has been proved to be very accurate and effective in the simulation of low Mach number viscous flows [13]. Upwind-biased differences are used for the convective terms, central differences for the viscous fluxes. Starting with a constant initialization of the scalar variables and body-fitted velocity components, the integration in time is carried out by a modified explicit Runge-Kutta time stepping as well as, optionally, an implicit Approximate-Factorization method (AF) or Symmetric-Gauss-Seidel (SGS) scheme.

2.1 Low Mach Number Modifications

Numerical algorithms for the simulation of compressible flows become inefficient and inaccurate at very low Mach numbers. The difficulties are due to the formulation of the governing equations in their discretized form. The problems have been addressed by many previous investigators, including Shuen *et al.* [10], Pletcher *et al.* [9] and Edwards *et al.* [1]. The main problem is the stiffness of the governing equations at low Mach numbers. The condition number of the Jacobian matrices (ratio of the maximal to the minimal eigenvalues) increases to infinity as the Mach number approaches zero. The time marching step therefore is restricted because of the large disparity of the eigenvalues of the Jacobian, representing the convective and acoustic signal speeds, respectively. The second problem results from the pressure singularity in the momentum equations at very low Mach numbers. The ratio of the magnitudes among the pressure term p and the convective terms ρu^2 is inversely proportional to the Mach number squared M^2. The large difference in magnitude will yield a large roundoff error.

To enable efficient numerical solutions of the equation system at low Mach number, a pseudo-time term is added to the time-dependent compressible Navier-Stokes equations. The primitive variables are employed as unknowns, rather than the traditional conservative variables. A preconditioning matrix Γ is used in order to eliminate the time-step difference between the convective and acoustic

characteristic speeds at low Mach number. The preconditioned equations can be discretized in the delta form:

$$\left[\Gamma + \frac{\Delta\tau}{\Delta t}\hat{A}_Q + \Delta\tau\left(\frac{\partial(\hat{A}_F)}{\partial\xi} + \frac{\partial(\hat{A}_G)}{\partial\eta} + \frac{\partial(\hat{A}_H)}{\partial\zeta}\right)\right]\Delta\hat{Q} = RHS\ ,$$

$$RHS = -\Delta\tau\left(\frac{\partial Q}{\partial t} + \frac{\partial F}{\partial\xi} + \frac{\partial G}{\partial\eta} + \frac{\partial H}{\partial\zeta}\right)\ , \tag{3}$$

where the Jacobian matrices are defined as,

$$\hat{A}_Q = \frac{\partial Q}{\partial\hat{Q}},\ \hat{A}_F = \frac{\partial F}{\partial\hat{Q}},\ \hat{A}_G = \frac{\partial G}{\partial\hat{Q}},\ \hat{A}_H = \frac{\partial H}{\partial\hat{Q}}\ . \tag{4}$$

Here Q is the vector of the conservative variables and $\hat{Q}$ is the vector of the primitive variables $(p, u, v, w, T)^T$. A more detailed description of the matrix Γ can be found in [14]. To circumvent the problem of large difference in magnitude of the convective and pressure terms in the momentum equations, a gradient splitting of the Euler flux into convective terms and a pressure term can be considered:

$$\nabla(\rho u^2 + p) = \nabla(\rho u^2) + \nabla p. \tag{5}$$

Both split gradients are of the same order of magnitude, independent of the Mach number. The Liou's Advection Upwind Splitting Method is applied to treat the convective and pressure terms separately. The convective terms are upstream-biased using an appropriately defined advection Mach number at the cell interface, while the pressure term is strictly dealt with by using acoustic waves. One of the advantages of the method is that the upwind effect can be easily reached with few modifications of the programs.

2.2 Boundary Conditions

For the inlet and outlet planes of the simulated pipes, subsonic quasy one-dimensional non-reflecting boundary conditions were implemented. These were based on the Riemann invariants normal to the pipe cross-section.

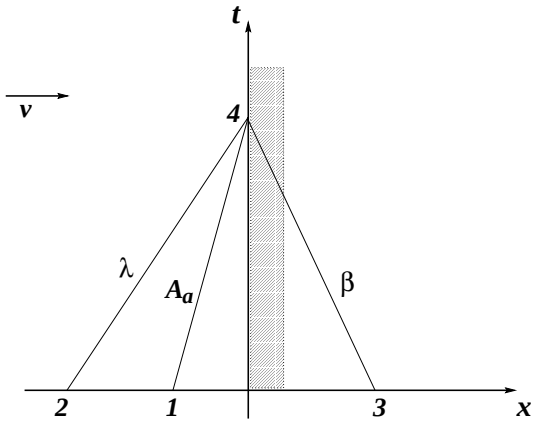

Figure 2. Characteristics at the free stream boundary.

For a one-dimensional partial differential equation in direction normal to the boundary:

$$Q_t + F_n = 0 \,, \tag{6}$$

the characteristics are:

$$\lambda = c + \frac{\gamma - 1}{2} u_n \qquad \text{corresponding to the direction} \qquad \frac{dn}{dt} = u_n + c \tag{7}$$

and

$$\begin{aligned} \beta &= -c + \frac{\gamma - 1}{2} u_n & \frac{dn}{dt} &= u_n - c \\ A_a &= c \left(\frac{p}{p_{ref}} \right)^{\frac{1-\gamma}{2\gamma}} & \frac{dn}{dt} &= u_n \end{aligned} \tag{8}$$

with u_n the velocity in direction normal to the boundary, n the normal coordinate, c the local speed of sound and γ the specific heat ratio. A_a is the speed of sound corresponding to some reference pressure p_{ref}. Similarly to enthalpy, A_a represents a state variable and remains constant along the particle path $1-4$. For isentropic flow A_a remains always constant. λ and β are the corresponding Riemann invariants. The characteristics for point (4) in figure 2 are:

$$\begin{aligned} A_{a4} &= A_{a1} + u_1 \frac{A_{a2} - A_{a1}}{c_2 - u_1} \\ \lambda_4 &= \lambda_2 + \left(\frac{\lambda + \beta}{2} \right)_2 \frac{A_{a4} - A_{a2}}{A_{a2}} \\ \beta_4 &= \beta_3 + \left(\frac{\lambda + \beta}{2} \right)_3 \frac{A_{a4} - A_{a3}}{A_{a3}} \,. \end{aligned} \tag{9}$$

With the help of A_a, λ, β known at the point (4), the conservative variables can be determined. The above boundary conditions made the pressure waves and other disturbances run out of the domain without any noticeable reflection. The interzonal boundary conditions enabled data exchange among the blocks of the computational grid and were accomplished by overlapping grids; at the walls, the no-slip solid viscous wall boundary conditions were used.

2.3 Turbulence Model

The highly complex geometrical and physical configurations are making the choise of an appropriate turbulence model very difficult. In the vortical, periodically separating flow with strong local rates of acceleration, any isotropic models are not adequate. The present authors decided, therefore, the use of the concept of large eddy simulation (LES).

2.4 Verification

The present numerical algorithm was subjected to verification of it's temporal and spatial accuracy and consistancy. The scheme is formally second order accurate in space, since the viscous terms are obtained from second order central differences. The scheme was first verified using the usual grid refinement study for the case of viscous flat plate flow at a free stream Mach number of $M_\infty = 0.5$. Defining the global error as the L_2 - norm of the deviation of the present solution from the Blasius

solution, second order accuracy was verified [12]. Next, the combination of the present solution scheme with the computational grid was investigated for the case of an optimized bluff body shape using three different grids. Figure 3 shows the density plot and summarizes the results. It should be noted that the finest grid very closely approaches the Strouhal number of the corresponding experiment.

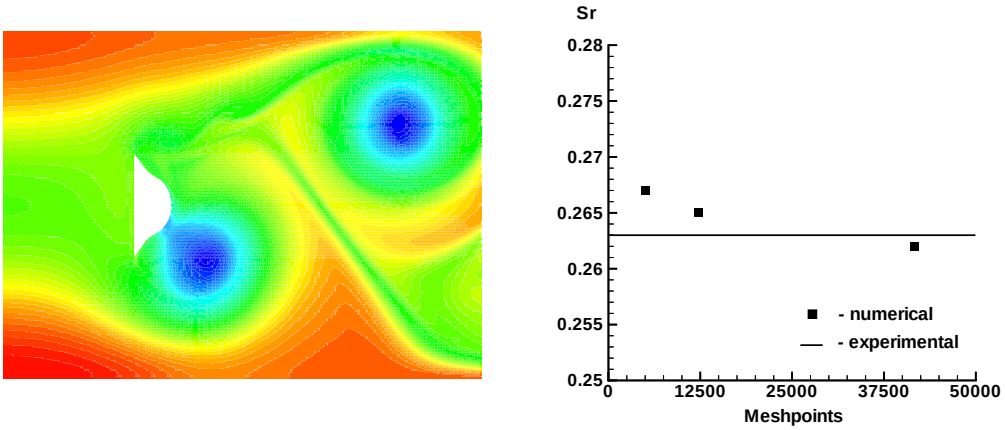

Figure 3. Grid refinement study for an optimized bluff body shape.

The temporal accuracy was tested by simulating 2-D flow about a cylinder, with free stream Mach number $M_\infty = 0.1$ and a Reynolds number of $Re = 200$. The resulting Strouhal number of the vortex separation is $Sr = 0.194$ and therefore within the range given in literature.

3 RESULTS

Figure 4 shows two basic strategies of mounting the bluff body inside a vortex-shedding flowmeter. The left device causes the separation of periodic vortices from the upper and lower edge of a bluff body, similar to the well known von Kármán vortex street. The right one produces axially-symmetric rings in the wake of a bluff body.

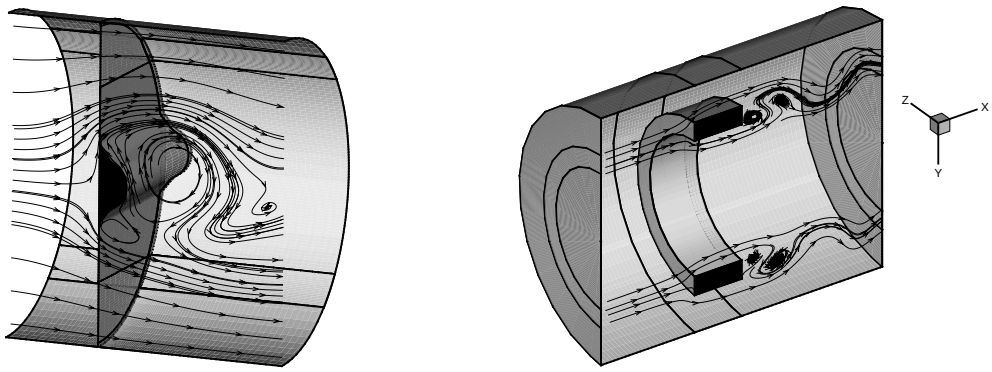

Figure 4. Two different designs of bluff body mounting inside a pipe.

As long as the inflow remains undisturbed, the shedding frequency in the wake of the bluff body is rather constant for most shapes. There are many studies concerning the optimization of the bluff body shapes, investigated under the condition of undisturbed inflow. We decided to examine the development of the vortex-shedding frequency in a more practical view. Flow meters are normally part of a pipe system and therefore the inflow is often nonuniform or even unsteady. Figure 5 shows the comparision of the shedding frequencies for undisturbed inflow (left) and flow downstream a single bend (right) using a DFT analysis.

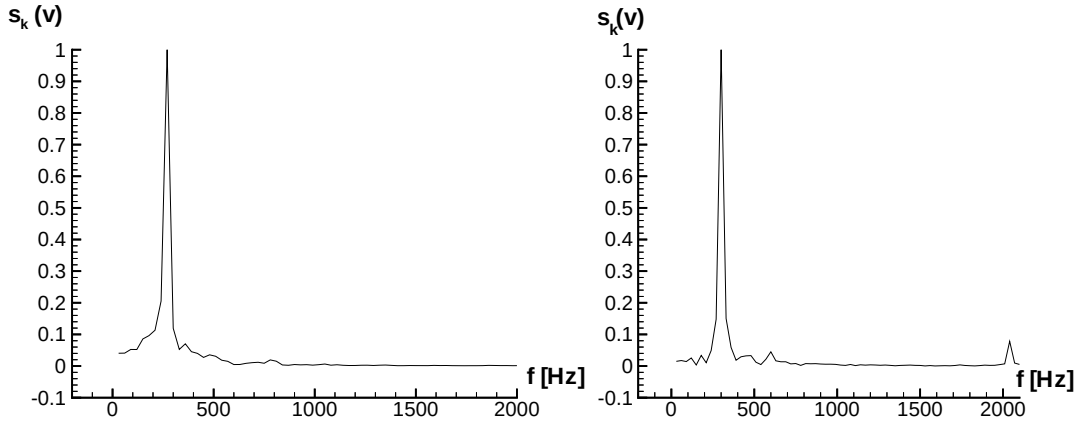

Figure 5. Shedding frequency for undisturbed inflow and flow downstream a single bend.

Figure 5 shows the result of DFT analysis of the flow behind the bluff body. On the left, the undisturbed flow is shown, displaying a very strong peak at the meter's natural vortex-shedding frequency. On the right, a result is shown after introducing a single bend upstream of the meter. In this case, the dominating frequency remains unchanged.

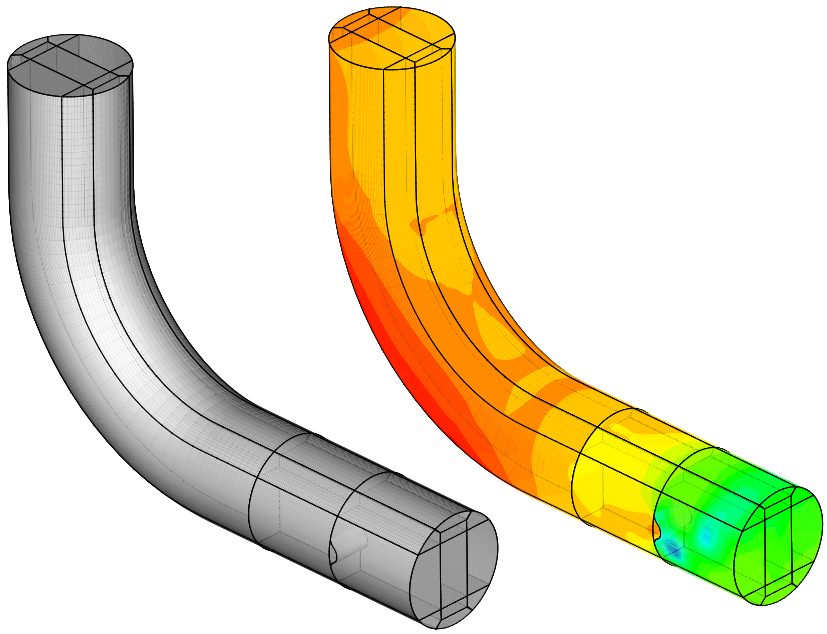

Figure 6. Pipe section and pressure contours.

In Figure 6, a section of the pipe, with a single bend and the protruding bluff body is shown, together with pressure contours at one time instant. The simulations are carried out under the following conditions.

Flow parameters:

- Pipe diameter D = 0.1 m,
- Mach number M = 0.1,
- Reynolds number Re = 225000,
- Prandtl number Pr = 0.7.

Numerical parameters:

- 33 block grid,
- 620000 mesh points.

Figure 7 shows the DFT analysis of flow with constant swirl upstream the meter. This condition is similar to the swirl produced downstream a double bend, Figure 8. Again, a very strong peak at the meter's frequency is noticeable.

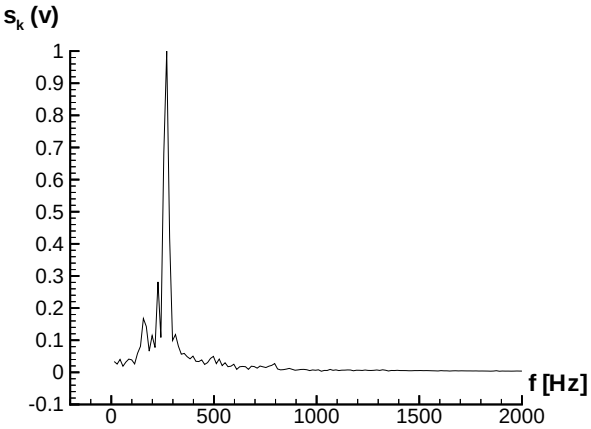

Figure 7. Shedding frequency for flow with constant swirl upstream the meter.

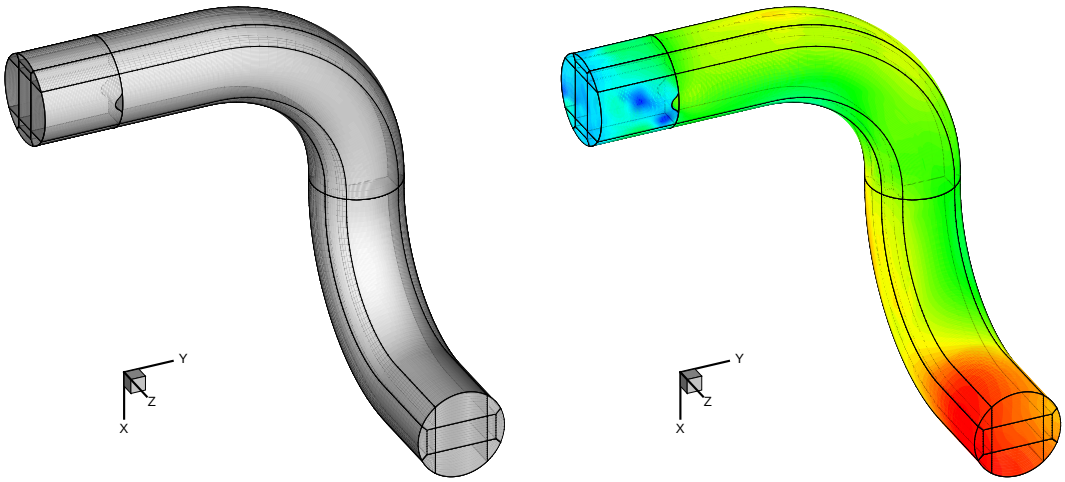

Figure 8. Shaded mesh and pressure contours of the double bend.

Figure 8 shows the mesh and the pressure contours of a double bend out of plane. The vortex street in the wake of the bluff body is well-defined, however, the simulation has not obtained enough periods of vortex-shedding to compute a DFT yet. It is assumed that it will be similar to the one with constant swirl upstream the meter, Figure 7.

4 CONCLUSIONS

Some numerical investigations of unsteady and disturbed pipe flow are presented. Therefore a verified and validated Navier-Stokes solver for three-dimensional simulations of compressible, viscous and unsteady flow is introduced. The simulations are very close to practical demands concerning the installation of the meter. The DFT analysis show that the vortex-shedding flowmeter will still work properly under these conditions.

5 ACKNOWLEDGEMENT

This work was supported by the *Deutsche Forschungsgemeinschaft* (DFG).

REFERENCES

[1] J. R. Edwards and C. J. Roy, AIAA Journal, Vol. 36, No. 2, pp. 185-192, 1998.
[2] C. Fureby, *Large-eddy simulation of turbulent anisochoric flows*, AIAA Journal, Vol. 33, No. 7, pp. 1263-1272, 1995.
[3] Hans, V., Poppen, G., Lavante, E. v., Perpeet, S. , *Interaction between vortices and ultrasonic waves in vortex-shedding flowmeters*, FLUCOME '97, Hayama, (1997).
[4] Hans, V., Poppen, G., Lavante, E. v., Perpeet, S., *Vortex-shedding flowmeters and ultrasound detection: signal processing and bluff body geometry*, Flow Measurement and Instrumentation 9 (1998), 79-82.
[5] Jameson, A., Schmidt, W., Turkel, E., *Numerical solutions of the Euler equations by finite volume methods using Runge-Kutta time-stepping schemes*, AIAA Paper, (81-1259), 1981.
[6] Johnson, M.W., *Computation of flow in a vortex-shedding flowmeter*, Flow Measurements and Instrumentation, 1:201-208, 1990
[7] Madabhushi, R.K., Choi, D., Barber, T.J., *Unsteady simulations of turbulent flow behind a triangular bluff body*, AIAA Paper, (97-3182), 1997.
[8] Miau, J.J., Yang, C.C., Chou, J.H. and Lee, K.R., *A T-shaped vortex shedder for a vortex flowmeter*, Flow Measurement and Instrumentation, Vol. 4, No. 4, 259 - 267, 1993.
[9] R. H. Pletcher and K.-H. Chen, AIAA-93-3368-CP.
[10] J.-S. Shuen, K.-H. Chen, and Y. Choi, J. of Comp. Phy. 106, pp. 306-318, 1993.
[11] Vatsa,V.N.,Thomas,J.L.,Wedan,B.W., *Navier-Stokes computations of prolate spheroids at angle of attack*, AIAA Paper, (87-2627), 1987.
[12] von Lavante, E., *The Accuracy of Upwind Schemes Applied to the Navier-Stokes Equations*, AIAA Journal, Vol. 28, No. 7, 1990.
[13] von Lavante, E., Yao, J., *Simulation of flow in exhaust manifold of an reciprocating engine*, AIAA 24th Fluid Dynamics Conference, 1983.
[14] J. Yao and E. von Lavante, Proceedings of 7th International Symposium on CFD, pp. 689-694, Sept. 15-19, 1997, Beijing, PR China.
[15] Hans, V., Windorfer, H., von Lavante, E. and Perpeet, S., *Experimental and numerical optimization of acoustic signals associated with ultrasound measurement of vortex frequencies*, Proceedings of FLOMEKO '98, 1998.

AUTHOR(S): Prof. Dr.-Ing. Ernst von Lavante, Dr.-Ing. Stephan Perpéet, Institute of Turbomachinery, Prof. Dr.-Ing. Volker Hans, Dipl.-Ing. Harald Windorfer, Institute of Measurement and Control, University of Essen, 45127 Essen, Germany, phone +49 (0)201-183-2901. E-mail: erni@tigger.turbo.uni-essen.de, stephan@tigger.turbo.uni-essen.de.